On the Oxenoid Character of Alkylperoxy Anions and Their Lithium Compounds: A Combined Mass-Spectrometric and Theoretical Investigation

Christoph A. Schalley[a], Detlef Schröder[a], Helmut Schwarz*[a], Konrad Möbus[b], and Gernot Boche*[b]

Institut für Organische Chemie der Technischen Universität Berlin[a],
Straße des 17. Juni 135, D-10623 Berlin, Germany

Fachbereich Chemie der Philipps-Universität[b],
D-35032 Marburg, Germany

Received March 24, 1997

Keywords: Mass spectrometry / Peroxides / Oxenoids / Density functional theory / Kinetic energy release

A combined mass-spectrometric and theoretical approach has been used for an investigation of the gas-phase chemistry of two representative alkylperoxy anions. Metastable CH_3OO^- ions undergo unimolecular loss of molecular hydrogen and formaldehyde yielding HCO_2^- and OH^-, respectively. The observed reactivity is in pleasing agreement with calculations of the $[C,H_3,O_2]^-$ and $[C,H,O_2]^-$ potential-energy surfaces at the BECKE3LYP/6-311++G** level of theory. Upon exhaustive methylation of the α-position as in t-$C_4H_9OO^-$ anions, the reactivity switches completely to an elimination of $(CH_3)_2C{=}CH_2$ giving rise to the formation of HOO^-. The results obtained for the "bare" alkylperoxy anions are used for the analysis of the EI mass spectrum of $(t$-$C_4H_9OOLi)_{12}$ dodecamers, which thermally decompose in the inlet system at a probe temperature of ca. 130°C. The decomposition is rationalized by a mechanism involving nucleophilic attack of one t-C_4H_9OOLi subunit on the oxenoid oxygen atom of a second t-C_4H_9OOLi moiety. This reaction may produce t-C_4H_9OOOLi trioxy species as intermediates, which rapidly decompose to singlet dioxygen and t-C_4H_9OLi.

Introduction

Lithium[1] and magnesium[2] salts of hydroperoxides reveal some intriguing features as far as reactivity, structural, and electronic properties are concerned. In analogy to isoelectronic carbenoids, $R'_2C(OR)Li$[3–5], and nitrenoids, $R'N(OR)Li$[6,7], the hydroperoxide salts can be regarded as oxenoids O(OR)Li (Scheme 1). Consequently, for oxenoids we can expect analogous reactions to those observed for carbenoids and nitrenoids[3–7]; in fact, they readily react as electrophiles with nucleophiles such as Grignard reagents or alkyl lithium compounds to yield metal alkoxides[1,8]. The nucleophilic attack is supported by the favorable energy of the σ^*_{O-O} orbital[1c]. Recently[1e], the structure of lithiated *tert*-butyl hydroperoxide, t-C_4H_9OOLi (**1**), has been determined by X-ray crystallography to be a dodecamer $(\mathbf{1})_{12}$. The lithium ions bridge the two oxygen atoms of each alkylperoxy subunit, and ab initio calculations support this feature[1e]. Similar structures have been calculated earlier for transition metal containing systems like $(HO)_3TiOO$-t-C_4H_9 and $(H_2N)_2FeOOH$[1c,9], which have been suggested to play key roles as catalysts in organic syntheses[10], for example in the Sharpless epoxidation[11]. The oxenoid character of peroxy anions is reflected in the O–O bond lengths, which are significantly elongated due to increased repulsion of the lone pairs. For example, this bond is as long as 1.479 Å (see below[12]) for CH_3OO^- ($\mathbf{2}^-$) as compared to the neutral $CH_3OO^\bullet$ radical $\mathbf{2}^\bullet$ (1.318 Å). This holds also true for other calculated species such as LiOOH[1c,9] and experimentally characterized structures[1e]. Of course, aggregation effects may well play an important role for the actual bond lengths of $(\mathbf{1})_{12}$ in the solid phase[1c].

Scheme 1

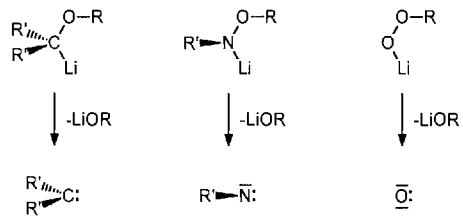

In the course of a mass-spectrometric characterization of $(\mathbf{1})_{12}$ by conventional electron ionization (EI), a mass spectrum (Figure 1) was obtained, which surprisingly contains signals for mixed oligomeric $(t$-$C_4H_9OLi)_m(t$-$C_4H_9OOLi)_nLi^+$ $(m + n = 1-8)$ cluster ions, which are due to formal losses of oxygen atoms from $(t$-$C_4H_9OOLi)_{m+n}Li^+$ ions. The base peak of the spectrum corresponds to protonated acetone (m/z = 59), a typical fragmentation product of species bearing t-C_4H_9O units. The structural assignment of these ions is supported by the observation of an intense signal for acylium ions (m/z = 43). Thus, all ions observed in the EI mass spectrum of $(\mathbf{1})_{12}$ can easily attributed to fragments of $(\mathbf{1})_{12}$ and are closed-shell species. However, the cluster ions observed in the mass range m/z = 1000–1100 form a notable exception. They cannot be explained by closed-shell cluster ions held together by one additional Li^+ ion. Instead, they correspond

  0009–2940/97/0808–1085 $ 17.50+.50/0

Figure 1. EI (70 eV) mass spectrum of $(\mathbf{1})_{12}$ at a probe temperature of ca. 130°C; insct: mass range of m/z = 500 to 1100 amplified by a factor of 40 relative to the original spectrum; note that not all cluster ions are visible due to suppression of very weak signals by the detection threshold of the instrument

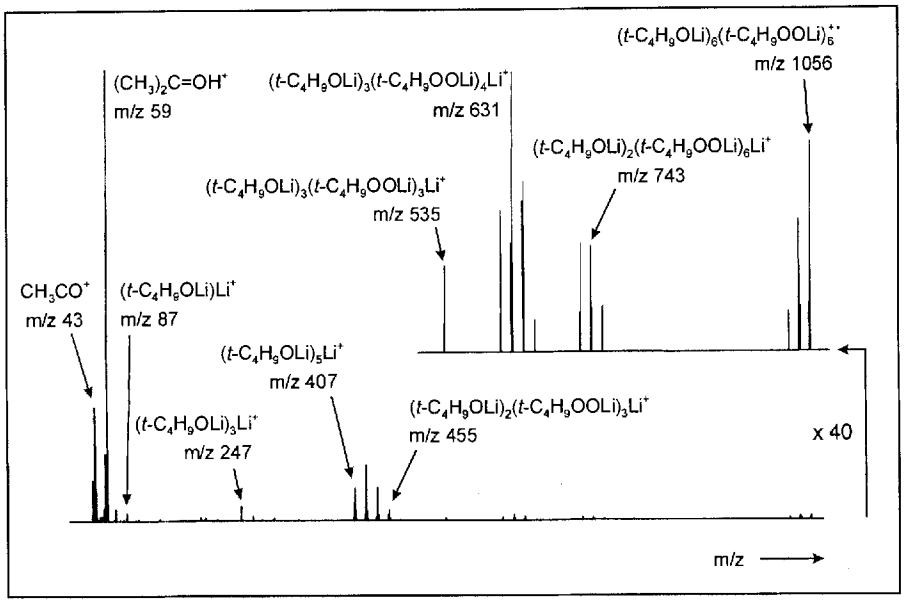

to the products of formal oxygen atom losses from cation radicals of dodecameric $(\mathbf{1})_{12}$. Hence, the signal at, for example, m/z = 1056 corresponds to $(t\text{-}C_4H_9OLi)_6(t\text{-}C_4H_9OOLi)_6^{+\bullet}$. Note that signals for clusters with higher masses such as the $(t\text{-}C_4H_9OOLi)_{12}^{+\bullet}$ molecular ion are suppressed by the detection threshold of the instrument. In fact, the formation of open-shell clusters exclusively for the dodecamers strongly supports the presence of genuine dodecamers as derived from X-ray crystallographic analysis[1e].

As far as the oxenoid character of metallated hydroperoxides is concerned, several questions arise from these findings: (i) What is the mechanistic origin of the formal O-atom expulsion? Does it reflect the oxenoid character of metallated hydroperoxides within the cluster ions? (ii) The loss of an oxygen atom is quite endothermic by ca. 94 kcal/mol for the model reaction $HOO^- \rightarrow HO^- + {}^1O$ and is still quite unfavorable (ΔH_r = +49 kcal/mol), if a spin-forbidden generation of triplet oxygen atoms is assumed[13]. Thus, is a unimolecular gas-phase reaction feasible? (iii) Does the metal ion support the elimination of oxygen atoms? (iv) If the formal oxygen atom loss does not occur as unimolecular gas-phase process, how are the corresponding ions formed? What, for example, is the conceivable role of thermal decomposition of the solid probe in the inlet system of the mass spectrometer? (v) If so, what is then the mechanism of this reaction? These and related questions will be addressed in the present article. In order to obtain more detailed insight into the gas-phase chemistry of alkylperoxy anions, we have conducted combined mass spectrometric[14] and theoretical investigations on two representative examples, i.e. "bare" CH_3OO^- and $t\text{-}C_4H_9OO^-$. These ions can easily be generated by negative ion chemical ionization (NICI) of a mixture of the corresponding alkyl hydroperoxides and N_2O. Extensive calculations for the $[C,H_3,O_2]^-$ and $[C,H,O_2]^-$ potential-energy surfaces at the BECKE3LYP/6-311++G** level of theory support the conclusions drawn from the experiments with methyl peroxy anions. Based on these results, the unusual mass spectrometric behavior of $(\mathbf{1})_{12}$ can be rationalized in terms of a thermal reaction in the solid phase prior to ionization. A plausible mechanism is proposed by which the decomposition may proceed.

Results and Discussion

Before discussing the mass-spectrometric behavior of alkylperoxy anions, let us first mention a fundamental point concerning the amount of internal energy, which can be stored in metastable anions decomposing on the μsec time scale of tandem mass spectrometric experiments[15]. Electron affinities (EA) of most organic molecules are usually quite low as compared to the energetic demand of rearrangement or dissociation reactions. For example, for larger alkoxy radicals EA values of 1.5 to 2.0 eV have been derived[13], and for hydrogen peroxy radicals HOO• a value of only 1.08 eV has been reported in the literature[13], which is below most of the typical bond dissociation energies. For metastable ion (MI) decompositions, any process involving barriers or exit channels above the threshold defined by the electron affinity can, therefore, not compete with electron detachment. However, upon activation of the anions in high-energy collisions[16], direct bond cleavages may yet occur quite efficiently. Thus, new processes become often visible in the CA mass spectra, which are "forbidden" for the metastable ions on energetic grounds. In addition, the total fragment ion currents are often enhanced; for example, the total ion current was higher by a factor of ca. 500 for the CA mass spectrum of methyl peroxy anions, $\mathbf{2}^-$, as com-

pared to its MI mass spectrum. These constraints have also to be kept in mind for the computational analysis; obviously, all transition structures and exit channels considered as relevant for the unimolecular decay must necessarily be located below the threshold defined by the respective electron affinities. Further, if exothermic rearrangements en route to products lead to intermediates, due to the huge amount of internal energy, these excited intermediates will exhibit a dissociation behavior which is closer to that of collisionally activated than that of metastable ions. As a result, direct bond cleavage and isomerization processes can efficiently compete with electron detachment. In other words, if unimolecular dissociation of a metastable anion proceeds via intermediates much more favorable in energy, the thermochemical threshold is defined by the electron affinity of the starting anion, while the EAs of intermediates do not necessarily play such an important role.

The Unimolecular and Collision-Induced Decay of Methyl Peroxy Anions

Figure 2 presents the MI and CA mass spectra of CH_3OO^- anions $\mathbf{2}^-$ generated by NICI of CH_3OOH withN_2O. Metastable $\mathbf{2}^-$ decomposes via two fragmentation pathways (Figure 2a): (i) Elimination of H_2 ($\Delta m = 2$) gives rise to a rather broad signal for $[C,H,O_2]^-$ anions. The kinetic energy released ($T_{0.5}$) in this process can be estimated[17] from the peak's half-height width, and a value of $T_{0.5} \approx 1.35$ eV has been derived. The amount of released energy is quite large and points to a significant barrier for the reverse reaction. (ii) Loss of formaldehyde ($\Delta m = 30$) results in the formation of OH^-. The signal for OH^- anions is characterized by its distinctly dished-topped peak shape[18] ($T_{0.5} \approx 1.22$ eV), leading again to the conclusion that a large amount of kinetic energy is released during the expulsion of formaldehyde.

Upon collisional activation (Figure 2b) three additional processes are observed: (i) The formation of $O_2^{-\bullet}$ by C–O bond cleavage corresponds to the base peak in the CA mass spectrum. From the absence of the $O_2^{-\bullet}$ signal in Figure 2a, one can conclude that collision processes do not contribute to the MI spectrum. Hence, the losses of dihydrogen and formaldehyde represent indeed unimolecular fragmentations of metastable anions. Furthermore, the presence of an intense signal for $O_2^{-\bullet}$ in the CA mass spectrum indicates that the major part of the ion beam consists of CH_3OO^- ions with an intact O–O bond. This structural assignment is further supported by charge reversal[19] and neutralization-reionization mass spectrometric experiments[20]. (ii) A very minor CH_3O^- fragment indicates the loss of an oxygen atom. (iii) Vice versa, $O^{-\bullet}$ contributes to the CA mass spectrum. The latter two reactions are indicative for O–O bond cleavage. Since they are not observed in the MI mass spectrum and are of low abundances in the CA spectrum, they are expected to be rather energy demanding. The fragmentations observed for CD_3OO^- anions are in complete agreement with these findings and therefore not reported here.

As far as the course of the fragmentations of metastable CH_3OO^- is concerned, a few alternatives are depicted in

Figure 2. (a) MI and (b) CA mass spectra of CH_3OO^- anions $\mathbf{2}^-$; note the pronounced dished topped peak for OH^- generation indicating a large kinetic energy release in the decomposition of CH_3OO^- into CH_2O and OH^-

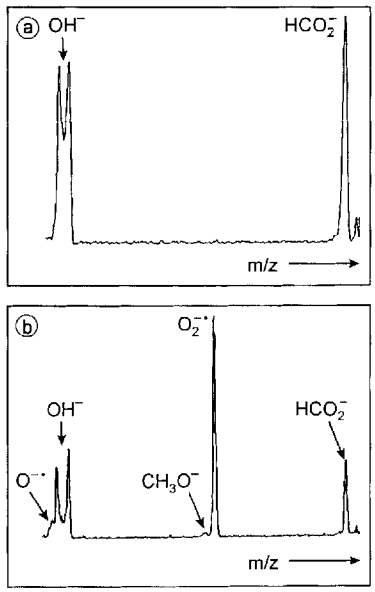

Scheme 2. The OH^- anions may be generated directly from $\mathbf{2}^-$ by a formal 1,2-elimination reaction. However, it is not so easy to explain the loss of dihydrogen from $\mathbf{2}^-$. This holds true in particular, if one considers the energetic threshold for electron detachment, which is only ca. 26 kcal/mol above the energy of the equilibrium geometry of $\mathbf{2}^-$ (see below). More likely, the H_2 elimination proceeds via an intermediate, for which deprotonated dihydroxy methane $\mathbf{3}^-$ represents a tempting structure. Assuming that $\mathbf{3}^-$ can be formed from $\mathbf{2}^-$ within the energetic constraints, the expulsion of H_2 can be described in terms of a 1,2-elimination, in course of which formation of the energetically favorable formiate anion $\mathbf{5}^-$ serves as a driving force.

Scheme 2

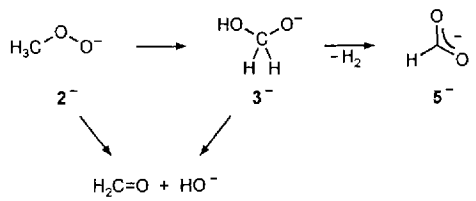

In order to obtain a more detailed insight into the mechanism and the energetics of the decompositions of $\mathbf{2}^-$ in the gas phase, high level DFT/HF calculations at the BECKE-3LYP/6-311++G** level of theory were performed. As demonstrated earlier, a large basis set is necessary for a reasonable description of electron affinities[22]. Quite fortunately, when compared to experimental electron affinities, the BECKE3LYP method gives much better data than the more costly MP2 approach with the same basis set applied (see below). The optimized geometries of $[C,H_3,O_2]^-$ isomers and transition structures are depicted in Chart 1. The energetic data (Tables I, 2) allow to construct the relevant

parts of the $[C,H_3,O_2]^-$ potential-energy surface (Figure 3). The peroxy anion CH_3OO^-, **2**$^-$, (ΔH_f = −20.0 kcal/mol) is located below the corresponding neutral by ca. 26 kcal/mol. The geometries of **2**$^-$ and **2**$^\bullet$ differ particularly with regard to the C−O and O−O bond lengths. Thus, the C−O bond is shorter (**2**$^-$: 1.386 Å, **2**$^\bullet$: 1.450 Å) for the anion, while the O−O bond is longer (**2**$^-$: 1.479 Å, **2**$^\bullet$: 1.318 Å). The calculated electron affinity of 1.14 eV for **2**$^\bullet$ nicely agrees with the literature value of HOO$^\bullet$ (1.08 eV)[13]. Hence, it can be assumed that our calculations are quite reliable and serve their purpose.

Chart 1

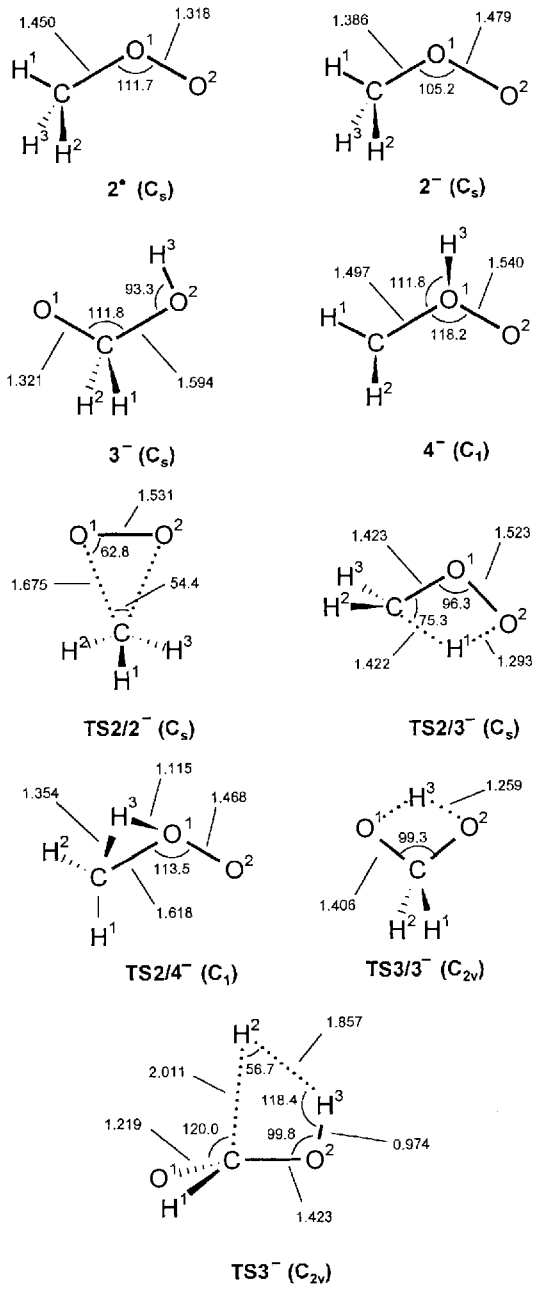

Three direct exit channels can be accessed from **2**$^-$: Methyl loss together with formation of $O_2^{-\bullet}$ is the lowest in energy ($\Sigma\Delta H_f$ = 19.5 kcal/mol), but yet it is located ca. 13 kcal/mol above the thermochemical threshold for electron detachment (ΔH_f = 6.2 kcal/mol). Generation of CH_3O^- + ^3O ($\Sigma\Delta H_f$ = 27.3 kcal/mol) and $CH_3O^\bullet$ + $O^{-\bullet}$ ($\Sigma\Delta H_f$ = 25.0 kcal/mol) are comparable in energy, but higher by additional 7 kcal/mol. Note that formation of triplet oxygen atoms is also spin-forbidden. These results are exactly in line with the experimental data presented above, as none of these fragments is observed in the metastable ion spectrum (Figure 2a); quite clearly, they cannot compete with elec-

Figure 3. $[C,H_3,O_2]^-$ potential-energy surface calculated at the BECKE3LYP/6-311++G** level of theory (ΔH_f values in kcal/mol)

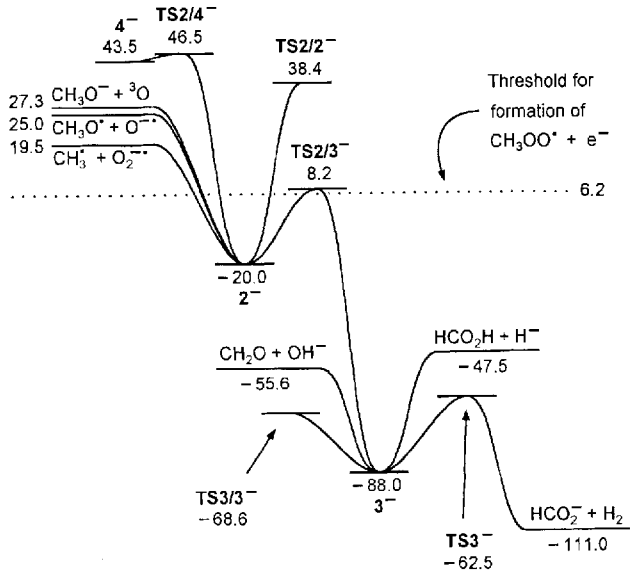

Table 1. Calculated total energies (E_{total}), zero-point vibrational energies (ZPVE), and calculated as well as experimental heats of formation (ΔH_f) of $[C,H_3,O_2]^{\bullet/-}$ isomers and relevant fragmentation reactions[a]

		E_{tot} [b] (hartree)	ZPVE (hartree)	ΔH_f [c] (kcal/mol)	ΔH_f [d] (kcal/mol)
$CH_3OO^\bullet$	**2**$^\bullet$	−190.235866	0.042718	6.2	2.4
CH_3OO^-	**2**$^-$	−190.277534	0.040806	−20.0	
$HOCH_2O^-$	**3**$^-$	−190.385877	0.041177	−88.0	
$CH_2O(H)O^-$	**4**$^-$	−190.176443	0.038356	43.5	
TS2/2$^-$		−190.184192	0.037363	38.4	
TS2/3$^-$		−190.232698	0.034847	8.2	
TS2/4$^-$		−190.171617	0.034532	46.5	
TS3/3$^-$		−190.355017	0.037729	−68.6	
TS3$^-$		−190.345259	0.035259	−62.5	
$HCO_2^- + H_2$		−190.422605	0.029948	−111.0	−111.0
$CH_2O + OH^-$		−190.334268	0.035028	−55.6	−58.8
$HCO_2H + H^-$		−190.321368	0.033307	−47.5	−55.8
$CH_3^\bullet + O_2^{-\bullet}$		−190.214605	0.032287	19.5	24.4
$CH_3O^- + {}^3O$		−190.202192	0.034502	27.3	27.1
$CH_3O^\bullet + O^\bullet$		−190.205185	0.036069	25.0	29.6
cyc-$CH_2O_2 + H^-$		−190.178095	0.032387	42.0	

[a] Calculated energies and literature heats of fragments are summarized in Table 2. — [b] Total energies based on BECKE3LYP/6-311++G** optimized structures including ZPVE corrections (unscaled). — [c] Calculated on the basis of literature data for the HCO_2^- + H_2 exit channel. — [d] Experimental data have been taken from ref.[13].

Table 2. Calculated total energies (E_{total}), zero-point vibrational energies (ZPVE), and experimental heats of formation (ΔH_f) of fragments

	E_{tot} [a] (hartree)	ZPVE (hartree)	ΔH_f [b] (kcal/mol)	ΔH_f [c] (kcal/mol)
H$^\bullet$	–0.502257	–		52.1
H$^-$	–0.534166	–	32.1	34.7
H_2	–1.169500	0.010072		0.0
^3O	–75.089880	–		59.6
^1O (^1D state)				104.5[e]
O$^{-\bullet}$	–75.149014	–	22.5	25.9
OH$^\bullet$	–75.753967	0.008445		9.3
OH$^-$	–75.818918	0.008530	–31.5	–32.8
$^3O_2$	–150.366693	0.003719		0.0
$^1O_2$ ($^1\Delta_g$ state)				22.6[e]
$O_2^{-\bullet}$	–150.389052	0.002654	–14.0	–10.4
$CH_3^\bullet$	–39.825553	0.029635		34.8
CO	–113.344010	0.005041		–26.4
HCO$^\bullet$	–113.878377	0.012954		10.7
HCO$^-$	–113.893943	0.009923	0.9	–3.5
CH_2O	–114.515350	0.026498		–26.0
$CH_3O^\bullet$	–115.056175	0.036069		3.7
CH_3O^-	–115.112312	0.034502	–31.5	–32.5
CO_2	–188.635227	0.011688		–94.1
$CO_2^{-\bullet}$	–188.624879	0.008332	–87.6[d]	
HCOOH	–189.787202	0.033307		–90.5
cyc-CH_2O_2	–189.643929	0.032387	0.6	
Li^+	–7.284918	–		162.4
LiOH	–83.404231	0.013107		
CH_3OLi	–122.683077	0.040977		

[a] Total energies based on BECKE3LYP/6-311++G** optimized structures including ZPVE corrections (unscaled). – [b] Calculated on the basis of literature data for the corresponding neutral. – [c] Experimental data have been taken from ref.[13]. – [d] The electron affinity (EA) of linear CO_2 is slightly negative by ca. –6.5 kcal/mol; however; single-point calculations for bent CO_2 at the equilibrium geometry of the corresponding anion radical [r(CO) = 1.231 Å, $\measuredangle$OCO = 137.8°], predict a positive EA of 29.4 kcal/mol. – [e] Since BECKE3LYP calculations are problematic with the excited singlet states of oxygen atoms and molecules, the excitation energy of 1.967 eV and 0.98 eV relative to the triplet ground states have been added to the calculated energies for the triplet species; for data, see ref.[21].

tron detachment. However, upon collisional activation, these reaction channels are populated to some extent, and the relative intensities of the ionic products as derived from the CA mass spectrum roughly correlate with the energetics of these exit channels. Even higher in enery (ΔH_f = 38.4 kcal/mol), the transition structure **TS2/2**$^-$ for the degenerate 1,2-methyl migration has been located. This process proceeds with retention of the configuration at the carbon center (Chart 1). However, due to its high energy demand it does not play any role in the present experiments. Similarly, the 1,2-hydrogen migration via **TS2/4** , which gives rise to a shallow minimum for deprotonated methanol oxide **4**$^-$, is only of theoretical interest[23].

With regard to the losses of dihydrogen and formaldehyde, intermediate formation of **3**$^-$ appears attractive. Indeed, **3**$^-$ represents a deep minimum on the $[C,H_3,O_2]^-$ potential-energy surface **3**$^-$ is located 68 kcal/mol below **2**$^-$. Both minima are connected by **TS2/3**$^-$, for which the reaction coordinate has been followed by an IRC calculation[24]. This transition structure (ΔH_f = 8.2 kcal/mol) is located slightly above the threshold (6.2 kcal/mol) for electron detachment, but this tiny energy difference is within the error margins of the calculations. In addition, electron detachment is a vertical process, which may have an energy demand somewhat higher than given by the adiabatic electron affinity. Furthermore, the small absolute ion abundance of the MI mass spectrum may indeed point to the presence of electron detachment as a process competing with the rearrangement. Thus, it is quite plausible to assume that **TS2/3**$^-$ is within the energetic limiations. If the decompositions of **2**$^-$ do indeed proceed via **3**$^-$ as intermediate, the barrier for the reverse reaction **3**$^- \rightarrow$ **2**$^-$ amounts to ca. 96 kcal/mol; this energy is stored in **3**$^-$ and gives rise to the large kinetic energy releases found for the metastable transitions (see above). Several attempts failed to locate a transition structure, which combines a 1,1-elimination of molecular hydrogen from **2**$^-$ either with or without a concerted 1,2-migration of the outer oxygen atom to the carbon center. Thus, a direct pathway for the reaction **2**$^- \rightarrow$ **5**$^-$ + H_2 has not been further pursued.

From **3**$^-$, a degenerate intramolecular hydrogen transfer via **TS3/3**$^-$ (ΔH_f = –68.6 kcal/mol) and several fragmentation channels are accessible: Cleavage of the C–O bond leads to the formation of CH_2O and OH$^-$ ($\Sigma\Delta H_f$ = –55.6 kcal/mol). It should be noted that we did not succeed in locating a transition structure for a 1,2-elimination leading directly from **2**$^-$ to these products. For the loss of H_2, **TS3**$^-$ has been found at a heat of formation of ΔH_f = –62.5 kcal/mol, i.e. ca. 7 kcal/mol below the energy demand for the C–O bond cleavage. As simple bond cleavages usually are entropically favored over rearrangements, both processes can easily compete with each other and are both observed in the MI mass spectrum with considerable intensities. Interestingly, the geometry of **TS3** (Chart 1) resembles much that expected for expulsion of a hydride concomitant with formation of formic acid: Thus, population analysis reveals that 70% of the negative charge is located on the moving hydrogen atom. The C–H bond of the leaving hydrogen is elongated to more than 2 Å, while the O–H bond length is still rather short (0.974 Å) and the $\measuredangle H^2CO^1$ angle of 120 degrees roughly resembles an intramolecular case of the Bürgi-Dunitz-Lehn trajectory[25] for a nucleophilic attack at a sp^2-hybridized carbon atom. Consequently, one might argue that **TS3**$^-$ is better described as an intermediate structure en route to the generation of formic acid and a hydride anion. However, the energy of this exit channel is ca. 15 kcal/mol higher than **TS3**$^-$ and instead the hydride collapses with the acidic proton and H_2 is released. This conjecture is fully confirmed by an IRC calculation (Figure 4), which demonstrates that first the hydride ion moves away from the carbon center followed by a deprotonation of the hydroxyl group to yield H_2 and formiate ($\Sigma\Delta H_f$ = –111.0 kcal/mol).

In order to characterize experimentally the anionic product of the hydrogen loss, a CA mass spectrum of [**2** – H_2]$^-$ generated in the ion source[26] has been recorded (Figure

Figure 4. Intrinsic reacton coordinate for **TS3**$^-$ describing the H_2 loss from **3**$^-$ with formiate as ionic product

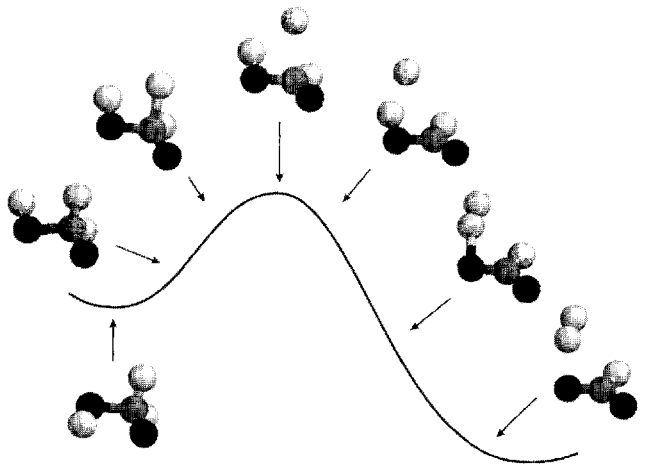

5). Three signals are observed: Besides minor signals for $O^{-\bullet}$ and OH^-, the anion radical of carbon dioxide represents the base peak. This result is somewhat surprising, because neutral CO_2 has a negative electron affinity of ca. -6 kcal/mol[27] and, therefore, is not expected to give rise to an anion radical at all. However, for a bent structure ($\measuredangle$OCO = 137.8°) a minimum has been located for the $CO_2^{-\bullet}$ anion radical[28], and apparently its lifetime is large enough to monitor it with mass spectrometric means. The CA mass spectrum depicted in Figure 5 is more or less identical with that of formiate anions **5**$^-$ (Chart 2) independently generated by NICI of formic acid with N_2O. However, there may well exist other $[C,H,O_2]^-$ isomers, which might lead to these CA mass spectral findings as well. In particular, hydroxy acyl anion **6**$^-$ represents a potential candidate, which upon H$^\bullet$ loss may give rise to a bent $CO_2^{-\bullet}$ anion radical as well. In addition, the weak OH^- signal in the CA mass spectrum of $[\mathbf{2} - H_2]^-$ ions can be easily rationalized to be generated from this isomer by simple C–O bond cleavage. Therefore, we studied the $[C,H,O_2]^-$ potential-energy surface theoretically[29].

Figure 5. CA mass spectrum of $[C,H,O_2]^-$ anions generated in the ion source from a mixture of methyl hydroperoxide and N_2O

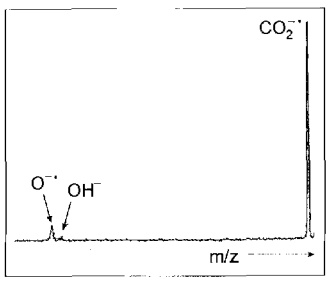

Formiate ions **5**$^-$ represent the most stable $[C,H,O_2]^-$ isomer ($\Delta H_f = -111.0$ kcal/mol, Table 3) on the $[C,H,O_2]^-$ potential-energy surface (Figure 6). Several other connectivities for the $[C,H,O_2]^-$ species **6**$^-$–**9**$^-$ (Chart 2) have been found to correspond to local minima (Chart 2). The high energy isomers **7**$^-$ and **8**$^-$, which bear a *cis*- or *trans*-$HCOO^-$ structure, are connected with deprotonated dioxirane **9**$^-$ via the transition structures **TS7/9**$^-$ and **TS8/9**$^-$ respectively. These species are far above any energetic limits and do not play any role in the unimolecular decay of CH_3OO^-. However, **6**$^-$ ($\Delta H_f = -73.3$ kcal/mol) and the transition structure **TS5/6**$^-$ ($\Delta H_f = -46.0$ kcal/mol) for the isomerization **5**$^-$ → **6**$^-$ are below the thermochemical threshold. Furthermore, the exit channel of lowest energy demand accessible from formiate **5**$^-$ corresponds to the formation of H^- + CO_2. Due to mass discrimikation effects, it is not visible in the mass spectrum. In addition, this process may be hampered by a significant barrier. Thus, upon collisional activation, **5**$^-$ can either decompose to H$^\bullet$ + $CO_2^{-\bullet}$ or rearrange via **TS5/6**$^-$. This barrier is located ca.

Chart 2

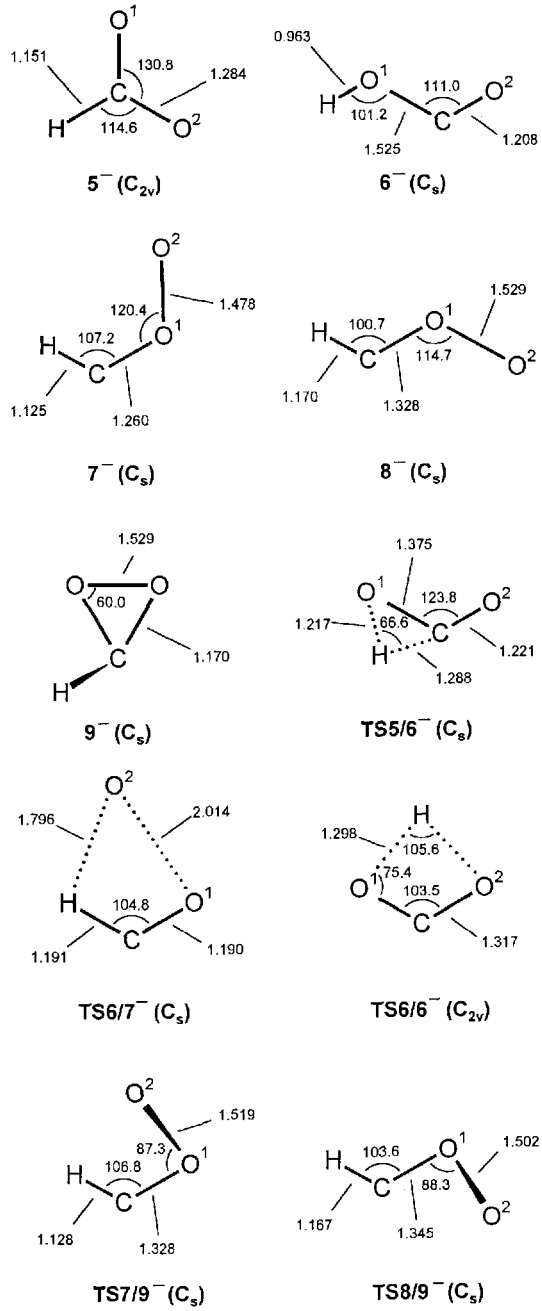

Figure 6. $[C,H,O_2]^-$ potential-energy surface calculated at the BECKE3LYP/6-311++G** level of theory (ΔH_f values in kcal/mol)

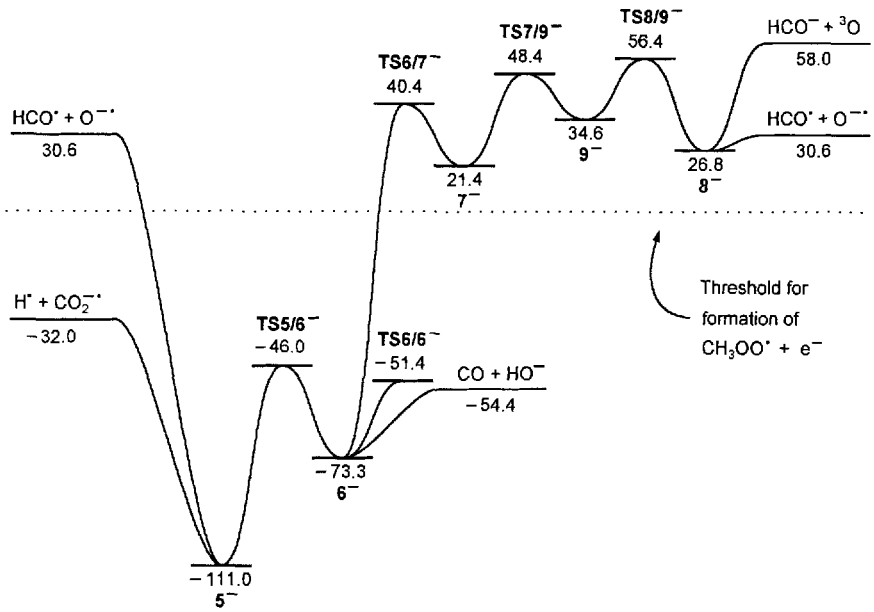

14 kcal/mol below the $H^\bullet + CO_2^{-\bullet}$ exit channel. In conclusion, formiate generated either from $\mathbf{2}^-$ by loss of H_2 or by NICI of formic acid can undergo collision-induced loss of $H^\bullet$ due to the favorable energetics, while some amount of C–O bond cleavage is visible as well. As high energy collisions increase the internal energy of the ions, a minor part of $\mathbf{5}^-$ ions can also rearrange to $\mathbf{6}^-$, which then gives rise to the weak OH^- signal in the CA mass spectrum of formiate.

Table 3. Calculated total energies (E_{total}), zero-point vibrational energies (ZPVE), and calculated as well as experimental heats of formation (ΔH_f) of $[C,H,O_2]^-$ isomers and relevant fragmentation reactions

		E_{tot} [a] (hartree)	ZPVE (hartree)	ΔH_f [b] (kcal/mol)	ΔH_f [c] (kcal/mol)
HCO_2^-	$\mathbf{5}^-$	−189.253105	0.019876	−111.0	−111.0
$HOCO^-$	$\mathbf{6}^-$	−189.193596	0.018686	−73.3	
cis-$HCOO^-$	$\mathbf{7}^-$	−189.042192	0.017050	21.4	
trans-$HCOO^-$	$\mathbf{8}^-$	−189.033532	0.016980	26.8	
cyc-HCO_2^-	$\mathbf{9}^-$	−189.021044	0.016952	34.6	
TS5/6$^-$		−189.149526	0.013841	−46.0	
TS6/6$^-$		−189.158095	0.014490	−51.4	
TS6/7$^-$		−189.011902	0.013159	40.4	
TS7/9$^-$		−188.999141	0.015290	48.4	
TS8/9$^-$		−188.986352	0.014213	56.4	
$CO + OH^-$		−189.162928	0.013571	−54.4	−59.2
$H^\bullet + CO_2^{-\bullet}$		−189.127136	0.008332	−32.0	
$HCO^\bullet + O^{-\bullet}$		−189.027391	0.012954	30.6	36.6
$HCO^- + {}^3O$		−188.983823	0.009923	58.0	56.1

[a] Total energies based on BECKE3LYP/6-311++G** optimized structures including ZPVE corrections (unscaled). – [b] Calculated on the basis of literature data for the formiate anion $\mathbf{5}^-$. – [c] Experimental data have been taken from ref.[13].

Finally let us discuss the transition structures **TS2/3**$^-$ (Chart 1) and **TS6/7**$^-$ (Chart 2) with respect to the oxenoid character of alkylperoxy anions. In both processes $\mathbf{2}^- \rightarrow \mathbf{3}^-$ and $\mathbf{6}^- \rightarrow \mathbf{7}^-$ an oxygen atom is formally inserted into a C–H bond. One might assume that these reactions are due to the oxenoid character, since oxenoid oxygen atoms should give rise to bond insertion as is observed for carbenes as well. However, this does not hold true for **TS2/3**$^-$ and **TS6/7**$^-$. Instead, the population analyses suggest that in both cases the major part of the negative charge is located on the moving oxygen atoms, which then deprotonate the hydrogen carbon bond. This results in formation of OH^-, which form new bonds to the electrophilic carbon centers to yield $\mathbf{3}^-$ and $\mathbf{7}^-$. In conclusion, there is no indication for the oxenoid character in the metastable and collision induced fragmentations of bare methyl peroxy anions.

The Gas-Phase Chemistry of *t*-$C_4H_9OO^-$ Anions

In order to proceed towards a more suitable model for the $(t\text{-}C_4H_9OOLi)_nLi^+$ complexes, we examined the completely α-methylated anion $\mathbf{10}^-$ ($t\text{-}C_4H_9OO^-$) and its fully deuterated isotopologue $\mathbf{10a}^-$. The MI and CA mass spectra are given in Figure 7. In the MI mass spectrum, HOO^- (m/z = 33) corresponds to the base peak, indicating an intact peroxidic structure; upon deuteration this signal is shifted to m/z = 34 for DOO^-. Most likely, isobutene is formed as neutral counterpart via a 1,2-elimination of HOO^-. Upon collisional activation a minor peak for $O_2^{-\bullet}$ becomes visible, but HOO^- formation continues to be the most abundant process. Two small signals at m/z = 71 and m/z = 73 correspond to the expulsions of water and methane. As methane is isobaric with atomic oxygen, one might assume that the signal at m/z = 73 belongs to oxygen losses and formation of $t\text{-}C_4H_9O^-$ anions. However, in the MI mass spectrum of $\mathbf{10a}^-$ no signal corresponding to oxygen atom losses is found at all. Thus, as already stated for the CH_3OO^- system, $t\text{-}C_4H_9OO^-$ anions also do not reveal

Figure 7. (a) MI and (b) CA mass spectra of t-$C_4H_9OO^-$ anions **10**$^-$

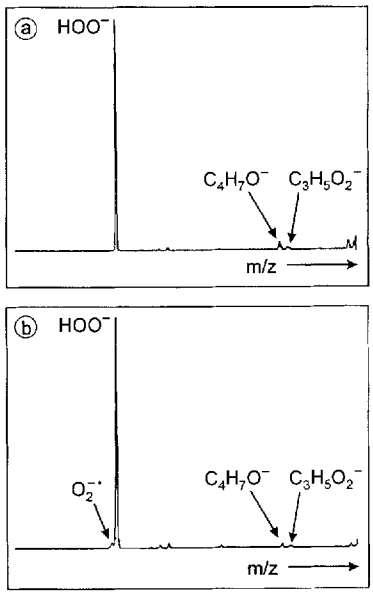

any indication for their oxenoid character as far as their unimolecular gas-phase chemistry is concerned.

Thermal Decomposition of the t-C_4H_9OOLi Dodecamer

Let us now return to the EI mass spectrum of $(\mathbf{1})_{12}$ (Figure 1). For comparison, lithium *tert*-butanolate has been characterized similarly by electron ionization (Figure 8). In agreement with earlier studies[30] on t-C_4H_9OLi and alkali halogenides and the EI mass spectrum of $(\mathbf{1})_{12}$, $(t\text{-}C_4H_9OLi)_xLi^+$ cluster ions are formed from t-C_4H_9OLi ($x = 1-7$)[31]. The $(t\text{-}C_4H_9OLi)_5Li^+$ pentamers represent the most abundant cluster ions in Figure 8. Their major decomposition reaction corresponds to the loss of $(t\text{-}C_4H_9OLi)_2$ dimers[30]. In close analogy, abundant pentameric $(t\text{-}C_4H_9OLi)_m(t\text{-}C_4H_9OOLi)_nLi^+$ ($m + n = 5$) are also formed from $(\mathbf{1})_{12}$.

Figure 8. EI (70 eV) mass spectrum of t-C_4H_9OLi at a probe temperature of ca. 150°C; the mass range of m/z = 420–600 is amplified by a factor of ten

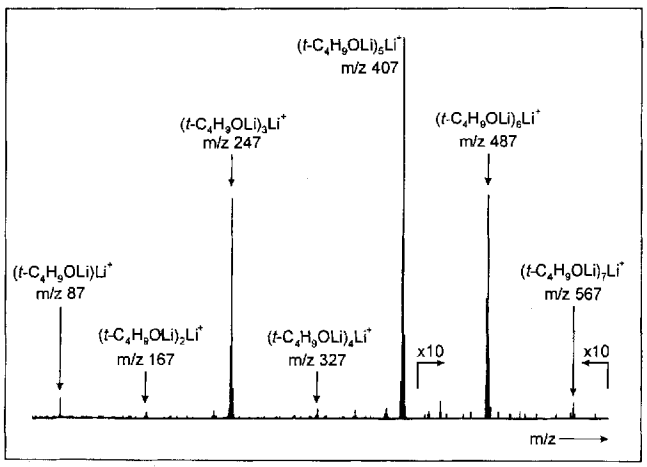

As far as the formal oxygen-atom losses from $(\mathbf{1})_{12}$ are concerned, the elemental composition has been examined for several clusters by analysis of the isotope distributions. Assuming natural isotope abundances, the distributions can be easily calculated and compared to the measured ones. Figure 9 displays the results for the $(t\text{-}C_4H_9OLi)_4(t\text{-}C_4H_9OOLi)Li^+$ (Figure 9a) and $(t\text{-}C_4H_9OLi)_5Li^+$ (Figure 9b) cluster ions. Indeed, the isotope patterns are those expected for consecutive losses of 4 and 5 oxygen atoms from $(t\text{-}C_4H_9OLi)_5Li^+$, respectively, rather than those calculated for consecutive losses of methane from the pentameric cluster.

Figure 9. Isotope distribution in (a) $(t\text{-}C_4H_9OLi)_4(t\text{-}C_4H_9OOLi)Li^+$ (m/z = 423) and (b) $(t\text{-}C_4H_9OLi)_5Li^+$ (m/z = 407) cluster ions as measured by scanning $B(1)$; the bold-line spectra give the isotope distributions calculated on the basis of natural isotope abundances

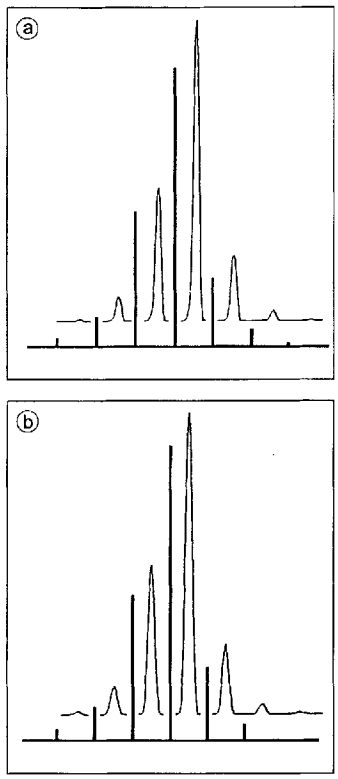

Nevertheless, with regard to the origin of the signals corresponding to formal oxygen atom losses, several arguments are not in line with the operation of such a process in the gas phase: (i) The CH_3OO^- and t-$C_4H_9OO^-$ model systems do not reveal any indication in favor of an oxenoid reactivity.

(ii) During the measurements of $(\mathbf{1})_{12}$, an exothermic, self-accelerating rection seems to occur in the solid sample of $(\mathbf{1})_{12}$ at temperatures of more than 130°C. Signal intensities and ion source pressure increase abruptly and last for several minutes, until the sample is consumed. Sometimes even a sudden decomposition of the solid has been observed.

(iii) As mentioned above, thermochemistry disfavors loss of atomic oxygen, because this is a highly endothermic reaction. It is, for example, not plausible to assume five con-

secutive oxygen atom expulsions for the pentameric $(t\text{-}C_4H_9OOLi)_5Li^+$ cluster, since each of them has an energy demand of at least ca. 50 kcal/mol. This would request an excess energy of more than 250 kcal/mol that had to be stored in a loosely bound cluster ion.

(iv) One might argue that complexation by lithium cations favors oxygen atom losses. This, however, would only be the case, if the $t\text{-}C_4H_9O\text{–}Li$ bond dissociation energy was much larger as compared to that of the $t\text{-}C_4H_9OO\text{–}Li$ bond. However, consideration of the model reactions (1) and (2) lead to comparable bond dissociation energies of 176.9 and 179.4 kcal/mol, such that we conclude that the metal ion does not influence much the thermochemistry of the oxygen loss.

$$CH_3OOLi \rightarrow CH_3OO^- + Li^+ \quad (1)$$

$$CH_3OLi \rightarrow CH_3O^- + Li^+ \quad (2)$$

(v) Unfortunately, the ion intensity of pentameric $(t\text{-}C_4H_9OOLi)_5Li^+$ was too low for performing MI or CA experiments, but we succeeded in recording a CA mass spectrum of $(t\text{-}C_4H_9OLi)_3\text{–}(t\text{-}C_4H_9OOLi)_2Li^+$ cluster ions (Figure 10). This cluster still contains two peroxidic subunits, and one would expect that oxygen atom losses should be visible at least upon collisional activation. Instead, these ions exhibit losses of neutral $(t\text{-}C_4H_9OLi)_2$ and $(t\text{-}C_4H_9O\text{-}Li)(t\text{-}C_4H_9OOLi)$ dimers, which agrees with the findings for the lithium *tert*-butanolate clusters (see above)[32]. The loss of a $(t\text{-}C_4H_9OOLi)_2$ unit is expected to be present in the spectrum as well, but it does not exceed the signal-to-noise ratio.

Figure 10. CA mass spectrum of $(t\text{-}C_4H_9OLi)_3(t\text{-}C_4H_9OLi)_2Li^+$ cluster ions (m/z = 439); note that sequential losses of oxygen atoms do not occur even upon collisional activation; it is not clear, whether the signal at m/z = 327 is an artifact or corresponds to the loss of C_8H_{16}, i.e. two butene units

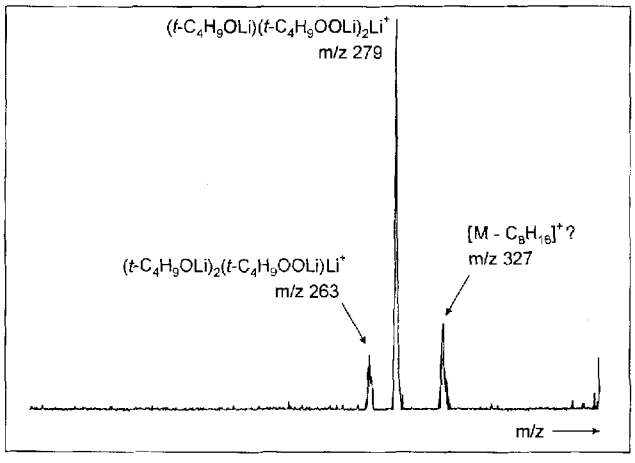

These overwhelming arguments rule out the possibility of oxygen-atom losses occuring in the gas phase. Thus, the observed cluster ions must be due to thermal decomposition of the solid and the question arises, what kind of mechanism is operative. As one is dealing with thermal activation, it is plausible to assume that molecular oxygen is generated instead of oxygen atoms. The analogy to carbenoids provides an idea about the mechanistic course of the reaction: It is known[33] that two $LiCH_2F$ molecules dimerize in ether solvents even at −100°C to ethene and 2 LiF, most probable via nucleophilic attack of one of the reaction partners on the carbenoid carbon atom of the other (Scheme 3a). Scheme 3b depicts an analogous mechanism for *tert*-butyl peroxy lithium **1** in the solid state. With lithium *tert*-butanolate as leaving group, in the first step one of the $t\text{-}C_4H_9OOLi$ molecules reacts with the oxenoid oxygen of the other. Formally, this process leads to an intermediate *tert*-butyl trioxylithium **11**[34], which is expected to easily decompose to singlet dioxygen and a second lithium *tert*-butanolate. Indeed, the formation of singlet dioxygen has been observed for the reaction of $Ti(Ot\text{-}C_4H_9)_4$ with $t\text{-}C_4H_9OOH$, in which alkylperoxo titanium species are proposed as intermediates[35].

Scheme 3

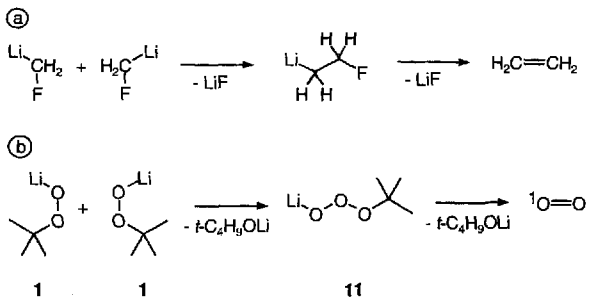

The proposed mechanism is in agreement with thermochemical considerations and calculations. As mentioned above, the model reaction $HOO^- \rightarrow HO^- + {}^1O$ is endothermic by ca. 94 kcal/mol. Instead, formation of $^1O_2$ from 2 HOO^- is essentially thermoneutral. The heat of reaction for 2 $HOO^- \rightarrow 2\ HO^- + {}^1O_2$ amounts to 1.4 kcal/mol[36]. These values can quite accurately be reproduced by calculations (Table 4), which result in ΔH_r = 91.2 and ΔH_r = −2.1 kcal/mol, respectively. The lithium ion in LiOOH does indeed support both the loss of oxygen atoms as well as the generation of molecular oxygen by some kcal/mol (Table 4). For the reaction $LiOOH \rightarrow LiOH + {}^1O$ a heat of reaction of ΔH_r = 84.1 kcal/mol has been calculated, which is lower than that of the bare anions by ca. 7 kcal/mol. Instead, the dimerization 2 $LiOOH \rightarrow 2\ LiOH + {}^1O_2$ is exothermic with ΔH_r = −16.3 kcal/mol instead of −2.1 kcal/mol for the HOO^- system. Similarly, the loss of a singlet oxygen atom from CH_3OOLi is endothermic by 89.7 kcal/mol, while the calculated heat of formation for the generation of $^1O_2$ is ΔH_r = −5.2 kcal/mol rendering the dimerization slightly exothermic. In contrast, the analogous dimerization of 2 $H_2C(F)Li$ to ethylene and 2 LiF has been calculated to be much more exothermic (ΔH_r = −98 kcal/mol[37]), while the reaction $H_2C(F)Li \rightarrow CH_2 + LiF$ has an endothermicity of ΔH_r = 49.3 kcal/mol. This accounts well for the experimental finding that $H_2C(F)Li$ cannot be isolated down to temperatures as low as −100°C[33], while $(\mathbf{1})_{12}$ does not decompose below a temperature of ca. 130°C.

Table 4. Calculated total energies (E_{total}), zero-point vibrational energies (ZPVE), and calculated relative energies for the oxygen atom and oxygen molecule losses from LiOOH and CH_3OOLi

	E_{tot} [a] (hartree)	ZPVE (hartree)	E_{rel} [b] (kcal/mol)	E_{rel}(Lit.) [c] (kcal/mol)
HOO^-	−150.982563	0.012912	0.0	0.0
$OH^- + {}^3O$	−150.908798	0.008530	46.3	49.1
$OH^- + {}^1O$ [d]			91.2	94.0
$2\,HOO^-$	−301.965126	0.025824	0.0	0.0
$2\,OH^- + {}^3O_2$	−302.004529	0.020779	−24.7	−21.0
$2\,OH^- + {}^1O_2$ [d]			−2.1	1.6
LiOOH	−158.556571	0.016947	0.0	
$LiOH + {}^3O$	−158.494111	0.013107	39.2	
$LiOH + {}^1O$ [d]			84.1	
2 LiOOH	−317.113142	0.033894	0.0	
$2\,LiOH + {}^3O_2$	−317.175155	0.026214	−38.9	
$2\,LiOH + {}^1O_2$ [d]			−16.3	
CH_3OOLi	−197.844290	0.044911	0.0	
$CH_3OLi + {}^3O$	−197.772957	0.040977	44.8	
$CH_3OLi + {}^1O$ [d]			89.7	
$2\,CH_3OOLi$	−395.688580	0.089822	0.0	
$2\,CH_3OLi + {}^3O_2$	−395.732847	0.085673	−27.8	
$2\,CH_3OLi + {}^1O_2$ [d]			−5.2	

[a] Total energies based on BECKE3LYP/6-311++G** optimized structures including ZPVE corrections (unscaled). – [b] Energies relative to the corresponding peroxidic species. – [c] Literature data has been taken from ref.[13]. – [d] Since BECKE3LYP calculations are problematic with the excited singlet states of oxygen atoms and molecules, the excitation energy of 1.967 eV and 0.98 eV relative to the triplet ground states have been added to the calculated energies for the triplet species; for data, see ref.[21].

Conclusions

The fragmentation mechanisms of methyl- and *tert*-butylperoxy anions in the gas phase can consistently be described by experiment and theory using the DFT/HF approach. Thus, within the energetic limit imposed by the electron affinity, methyl peroxy anion can rearrange to the energetically much more stable $HOCH_2O^-$ isomer. Due to cleavage of the peroxidic O–O bond, the latter ion is formed with ca. 96 kcal/mol of excess energy stored as rovibrational excitation. Similar effects have been found to influence the reactivity for a series of peroxidic species including cationradicals[38], protonated peroxides[39], and transition-metal complexes of peroxides[40]. Nevertheless, a particular oxenoid character of peroxy anions is not revealed in their unimolecular chemistry. Consequently, this feature is not an intrinsic property of alkyl peroxy anions and lithiated alkyl hydroperoxides; rather the presence of appropriate reaction partners plays a pivotal role.

These results can be transferred to the thermal decomposition of the *t*-C_4H_9OOLi cluster $(\mathbf{1})_{12}$. Thus, formal oxygen atom loss does not occur in the gas phase; rather, in the solid each peroxy anion reacts with a second one to liberate, most likely, singlet oxygen via a trioxy intermediate. Evaporation of the remaining mixture of *t*-C_4H_9OLi and *t*-C_4H_9OOLi accounts for the mixed cluster ions observed in the mass spectra of $(\mathbf{1})_{12}$. Thus, while a single peroxy unit does not behave like an oxenoid, the thermal decomposition of $(\mathbf{1})_{12}$ stresses the analogy between carbenoids and lithiated alkyl hydroperoxides[33]. Further studies dealing with the liberation of singlet dioxygen from ionic peroxides and the distinctly different thermochemistry of carbenoids and oxenoids are in progress.

We are grateful to *Jeremy Harvey*, Ph. D., for helpful comments and thank the *Deutsche Forschungsgemeinschaft* (SFB 260, SPP Peroxidchemie) and the *Fonds der Chemischen Industrie* for financial support.

Experimental Section

The experiments were performed using a modified VG ZAB/HF/AMD four-sector mass spectrometer of BEBE configuration (*B* stands for magnetic and *E* for electric sector) which has been described in detail previously[41]. Briefly, for the generation of the CH_3OO^- and *t*-$C_4H_9OO^-$ anions and their deuterated analogues, mixtures of N_2O and the hydroperoxides were ionized by negative ion chemical ionization (NICI)[42] in a chemical ionization source (repeller voltage ca. −0 V) with a beam of electrons having 50–100 eV kinetic energy. Note that a metal-free inlet system is necessary to reduce decomposition of the peroxides[40]. The ions of interest were accelerated to 8 keV translational energy and mass-selected by means of *B*(1) at a mass resolution of ca. $m/\Delta m = 2000$; isobaric impurities have not been observed. Unimolecular fragmentations of metastable ions (MI) occurring in the field-free region preceding *E*(1) were recorded by scanning this sector. For collisional activation (CA) experiments the ions were collided with helium in the same field-free region (80% transmission, T)[15]. In order to exclude artifacts[43], these experiments were repeated in the field-free region between *E*(1) and *B*(2), resulting in mass spectra of poorer quality, which, however, are in satisfying agreement with those obtained with *E*(1). HCO_2^- (DCO_2^-) anions generated in the ions source by either loss of molecular hydrogen from CH_3OO^- (CD_3OO^-) or by NICI of formic acid were analogously characterized by their CA mass spectra.

For EI mass spectra (70 eV electron energy, repeller voltage ca. 30 V), a small sample of $(\mathbf{1})_{12}$ was introduced via the heatable direct inlet system. The probe tip was heated very slowly to ca. 140°C, while the instrument was scanning. At ca. 130–135°C decomposition of the solid gives rise to sufficiently high ion currents of oligomeric ions $(t\text{-}C_4H_9OLi)_n(t\text{-}C_4H_9OOLi)_mLi^+$ (Figure 1) during a period of max. 5 minutes. This period was long enough for recording CA mass spectra (see above) of some of the most intense oligomers, which contained at least one peroxide subunit. In order to determine the exact elemental composition, *B*(1) scans were carried out to measure the isotope distribution.

The syntheses of methyl and [D_3]methyl hydroperoxides from dimethyl sulfate ([D_6]dimethyl sulfate) and aqueous hydrogen peroxide (10%) has been described earlier[44]. Unlabeled *tert*-butyl hydroperoxide was commercially available (70% aqueous solution) and used after purification (extraction with diethyl ether and removal of the solvent in vacuo). [D_9]*tert*-butyl hydroperoxide has been synthesized from [D_9]*tert*-butyl chloride and H_2O_2 using silver trifluoroacetate as coupling agent[45]. The synthetic procedure for $(\mathbf{1})_{12}$ has been described earlier[1e]. All substances were purified by well established laboratory procedures and identified by ^{1}H-NMR-spectroscopic and mass-spectrometric means.

Computational Details: All calculations were carried out with the BECKE3LYP DFT/HF hybrid method as implemented in the GAUSSIAN 94 program[46] using the BECKE3 parameter fit for atomization energies and the G2 set[47] for the ionization energies of

small molecules. The 6-311++G** basis set[48] was used for a proper description of anions[22]. The results obtained with the BECKE3-LYP method were compared to MP2 calculations with the same basis set applied and turned out to describe the electron affinities much better. For example, O_2 is predicted to have a negative electron affinity of ca. −0.5 kcal/mol with MP2, while the BECKE3LYP calculation results in +14 kcal/mol (experimental value: +10.4 kcal/mol)[13]. Geometry optimizations were performed by using gradient procedures. Vibrational frequencies were calculated in order to characterize stationary points as minima (no imaginary frequency) or transition structures (one imaginary frequency) and to account for zero-point vibrational energy (ZPVE) corrections. The ZPVE values reported in this study have not been scaled, since the scaling factors are close to unity for the BECKE3LYP method[49]. It is expected that this computational approach provides an accuracy of ca. ±5 kcal/mol[50]. If it was not obvious which minima are connected by a certain transition structure, the reaction path has been followed in Intrinsic Reaction Coordinate (IRC) calculations[24] at the same level of theory.

Appendix

For the sake of clarity, we reduced the calculated geometrical data presented in the Charts to the important features of the ion structures. Here, the complete set of data is given (bond lengths in Å, bond angles in °). Numbers of atoms are used as shown in the Charts.

$CH_3OO^•$, 2$^•$: C_s symmetry; $r(OO) = 1.318$; $r(CO^1) = 1.450$; $r(CH^1) = 1.089$; $r(CH^2) = 1.090$; $\angle CO^1O^2 = 111.7$; $\angle H^1CO^1 = 105.3$; $\angle H^2CO^1 = 109.0$; $\angle H^1CH^2 = 111.2$; $\angle H^2CH^3 = 110.8$; $\angle H^1CO^1O^2 = 180.0$; $\angle H^2CO^1O^2 = 60.6$.

CH_3OO^-, 2$^-$: C_s symmetry; $r(OO) = 1.479$; $r(CO^1) = 1.386$; $r(CH^1) = 1.104$; $r(CH^2) = 1.104$; $\angle CO^1O^2 = 105.2$; $\angle H^1CO^1 = 107.6$; $\angle H^2CO^1 = 111.5$; $\angle H^1CH^2 = 109.3$; $\angle H^2CH^3 = 107.4$; $\angle H^1CO^1O^2 = 180.0$; $\angle H^2CO^1O^2 = 60.1$.

$HOCH_2O^-$, 3$^-$: C_s symmetry; $r(O^1C) = 1.321$; $r(CO^2) = 1.594$; $r(CH^1) = 1.139$; $r(O^2H^3) = 1.002$; $\angle O^1CO^2 = 111.5$; $\angle H^1CO^1 = 118.7$; $\angle H^1CO^2 = 100.7$; $\angle H^1CH^2 = 103.8$; $\angle CO^2H^3 = 93.3$; $\angle H^1CO^2H^3 = 0.0$; $\angle O^1CO^2H^3 = 126.7$.

$CH_2O(H)O^-$, 4$^-$: C_1 symmetry; $r(OO) = 1.540$; $r(CO^1) = 1.497$; $r(CH^1) = 1.102$; $r(CH^2) = 1.103$; $r(O^1H^3) = 0.960$; $\angle CO^1O^2 = 118.2$; $\angle H^1CO^1 = 101.5$; $\angle H^2CO^1 = 105.6$; $\angle H^1CH^2 = 110.5$; $\angle CO^1H^3 = 111.8$; $\angle H^3O^1O^2 = 95.8$; $\angle H^1CO^1O^2 = -155.8$; $\angle H^2CO^1O^2 = 88.8$; $\angle H^1CO^1H^3 = 94.4$; $\angle H^2CO^1H^3 = -20.9$.

TS2/2$^-$: C_s symmetry; $r(OO) = 1.531$; $r(CO) = 1.675$; $r(CH^1) = 1.090$; $r(CH^2) = 1.133$; $\angle CO^1O^2 = 62.8$; $\angle O^1CO^2 = 54.4$; $\angle H^1CO^1 = 104.4$; $\angle H^2CO^1 = 92.6$; $\angle H^1CH^2 = 107.3$; $\angle H^2CH^3 = 101.9$; $\angle H^1CO^1O^2 = 97.7$; $\angle H^2CO^1O^2 = -153.6$.

TS2/3$^-$: C_s symmetry; $r(OO) = 1.523$; $r(CO) = 1.423$; $r(CH^1) = 1.105$; $r(CH^3) = 1.422$; $r(H^3O) = 1.239$; $\angle CO^1O^2 = 96.3$; $\angle O^1O^2H^3 = 77.3$; $\angle O^2H^3C = 111.1$; $\angle H^3CO^1 = 75.3$; $\angle H^1CO^1 = 111.0$; $\angle H^1CH^3 = 121.4$; $\angle H^1CH^2 = 110.3$; $\angle H^1CO^1O^2 = 118.5$; $\angle H^1CH^3O^2 = -106.0$; $\angle CO^1O^2H^3 = 0.0$.

TS2/4$^-$: C_1 symmetry; $r(OO) = 1.468$; $r(CO^1) = 1.618$; $r(CH^1) = 1.091$; $r(CH^2) = 1.096$; $r(CH^3) = 1.354$; $r(O^1H^3) = 1.115$; $\angle CO^1O^2 = 113.5$; $\angle H^1CO^1 = 102.5$; $\angle H^2CO^1 = 105.1$; $\angle H^1CH^2 = 110.7$; $\angle H^1CH^3 = 112.1$; $\angle H^2CH^3 = 131.1$; $\angle CO^1H^3 = 55.8$; $\angle H^3CO^1 = 42.9$; $\angle CH^3O = 31.2$; $\angle H^3O^1O^2 = 116.4$; $\angle H^1CO^1O^2 = -2.1$; $\angle H^2CO^1O^2 = -117.9$; $\angle H^1CO^1H^3 = -109.1$; $\angle H^2CO^1H^3 = 135.2$.

TS3/3$^-$: C_{2v} symmetry; $r(O^1C) = 1.406$; $r(CH^1) = 1.117$; $r(O^1H^3) = 1.259$; $\angle O^1CO^2 = 99.3$; $\angle CO^1H^3 = 72.1$; $\angle O^1H^3O^2 = 116.6$; $\angle H^1CO^1 = 112.5$; $\angle H^1CH^2 = 107.5$; $\angle H^1CO^1H^3 = 119.2$; $\angle O^1CO^2H^3 = 0.0$.

TS3$^-$: C_1 symmetry; $r(CO^1) = 1.219$; $r(CO^2) = 1.406$; $r(CH^1) = 1.094$; $r(CH^2) = 2.011$; $r(O^2H^3) = 0.974$; $r(H^2H^3) = 1.857$; $\angle O^1CO^2 = 120.3$; $\angle H^1CO^1 = 122.2$; $\angle H^1CO^2 = 112.7$; $\angle H^2CO^1 = 120.0$; $\angle H^1CH^2 = 82.0$; $\angle H^2CO^2 = 87.9$; $\angle CO^2H^3 = 99.8$; $\angle O^2H^3H^2 = 118.4$; $\angle H^3H^2C = 56.7$; $\angle CO^2H^3H^2 = -13.5$; $\angle H^1CO^2H^3 = -67.0$; $\angle H^1CH^2H^3 = 105.0$; $\angle O^1CO^2H^3 = 137.4$; $\angle O^1CH^2H^3 = -132.4$.

HCOOH: C_s symmetry; $r(CO^1) = 1.192$; $r(CO^2) = 1.354$; $r(CH^1) = 1.105$; $r(O^2H^2) = 0.966$; $\angle H^1CO^1 = 124.0$; $\angle H^1CO^2 = 113.5$; $\angle O^1CO^2 = 122.5$; $\angle CO^2H^2 = 109.8$; $\angle H^1CO^2H^2 = 0.0$; $\angle O^1CO^2H^2 = 180.0$.

***cyc*-CH_2O_2**: C_{2v} symmetry; $r(OO) = 1.501$; $r(CO) = 1.388$; $r(CH) = 1.090$; $\angle O^1CO^2 = 65.4$; $\angle CO^1O^2 = 57.3$; $\angle H^1CO^1 = 116.2$; $\angle H^1CH^2 = 116.8$; $\angle H^1CO^1O^2 = 108.4$.

HCO_2^-, 5$^-$: C_{2v} symmetry; $r(CO) = 1.284$; $r(CH) = 1.151$; $\angle HCO = 114.6$; $\angle OCO = 130.8$; $\angle HCOO = 180.0$.

HOCO$^-$, 6$^-$: C_s symmetry; $r(CO^2) = 1.208$; $r(CO^1) = 1.525$; $r(HO^1) = 0.963$; $\angle O^1CO^2 = 111.0$; $\angle HO^1C = 101.2$; $\angle HO^1CO^2 = 180.0$.

***cis*-HCOO$^-$, 7$^-$**: C_s symmetry, $r(HC) = 1.125$; $r(CO^1) = 1.260$; $r(OO) = 1.478$; $\angle HCO^1 = 107.2$; $\angle CO^1O^2 = 120.4$; $\angle HCO^1O^2 = 0.0$.

***trans*-HCOO$^-$, 8$^-$**: C_s symmetry, $r(HC) = 1.170$; $r(CO^1) = 1.328$; $r(OO) = 1.529$; $\angle HCO^1 = 100.7$; $\angle CO^1O^2 = 114.7$; $\angle HCO^1O^2 = 180.0$.

***cyc*-HCO_2^-, 9$^-$**: C_s symmetry, $r(HC) = 1.130$; $r(CO) = 1.478$; $r(OO) = 1.480$; $\angle HCO^1 = 102.8$; $\angle CO^1O^2 = 60.0$; $\angle O^1CO^2 = 60.0$; $\angle HCO^1O^2 = 97.6$.

TS5/6$^-$: C_s symmetry; $r(CO^1) = 1.375$; $r(CO^2) = 1.221$; $r(O^1H) = 1.217$; $r(CH) = 1.288$; $\angle O^1CO^2 = 123.8$; $\angle HCO^1 = 54.2$; $\angle CO^1H = 59.2$; $\angle O^1HC = 66.6$; $\angle HCO^2 = 178.0$; $\angle HO^1CO^2 = 180.0$.

TS6/6$^-$: C_{2v} symmetry; $r(CO) = 1.317$; $r(OH) = 1.298$; $\angle HOC = 75.4$; $\angle OHO = 105.6$; $\angle OCO = 103.5$; $\angle HOCO = 0.0$.

TS6/7$^-$: C_s symmetry; $r(CO^1) = 1.190$; $r(OO) = 2.014$; $r(CH) = 1.191$; $r(O^2H) = 1.796$; $\angle HCO^1 = 104.8$; $\angle CO^1O^2 = 92.4$; $\angle O^1O^2H = 59.0$; $\angle O^2HC = 103.9$; $\angle HCO^1O^2 = 0.0$.

TS7/9$^-$: C_1 symmetry; $r(HC) = 1.128$; $r(CO^1) = 1.328$; $r(OO) = 1.519$; $r(CO^2) = 1.969$; $\angle HCO^1 = 106.8$; $\angle CO^1O^2 = 87.3$; $\angle HCO^1O^2 = -62.3$.

TS8/9$^-$: C_1 symmetry; $r(HC) = 1.167$; $r(CO^1) = 1.345$; $r(OO) = 1.502$; $r(CO^2) = 1.986$; $\angle HCO^1 = 103.6$; $\angle CO^1O^2 = 88.3$; $\angle HCO^1O^2 = -121.2$.

[1] [1a] E. Müller, T. Töpel, *Ber. Dtsch. Chem. Ges.* **1939**, *72*, 273. – [1b] M.Julia, V. Pfeuty-Saint-Jalmes, J.-N. Verpeaux, *Synlett* **1993**, 233. – [1c] G. Boche, F. Bosold, J. C. W. Lohrenz, *Angew. Chem.* **1994**, *106*, 1228; *Angew. Chem. Int. Ed. Engl.* **1994**, *33*, 1161. – [1d] M. Julia, V. Pfeuty-Saint-Jalmes, K. Plé, J.-N. Verpeaux, G. Hollingworth, *Bull. Soc. Chim. Fr.* **1996**, *133*, 15. – [1e] G. Boche, K. Möbus, K. Harms, J. C. W. Lorenz, M. Marsch, *Chem. Eur. J.* **1996**, *2*, 604.

[2] [2a] V. Grignard, L. Lepaire, *Bull. Soc. Chim. Fr.* **1928**, *43*, 141. – [2b] C. Walling, S. A. Buckler, *J. Am. Chem. Soc.* **1955**, *77*, 6032. – [2c] G. Sosnovsky, J. H. Brown, *Chem. Rev.* **1966**, *66*, 529. – [2d] M. Maher-Detweiler in: Houben-Weyl, *Methoden der organischen Chemie*, Vol. E13/1, Thieme, Stuttgart, **1988**, p. 176.

[3] For reviews, see: [3a] G. Köbrich, *Angew. Chem.* **1967**, *79*, 15; *Angew. Chem. Int. Ed. Engl.* **1967**, *6*, 41. – [3b] W. Kirmse, *Carbene, Carbenoide und Carbenanaloge*, VCH, Weinheim, 1969. – [3c] G. Köbrich, *Angew. Chem.* **1972**, *84*, 557; *Angew. Chem. Int. Ed. Engl.* **1972**, *11*, 473.

[4] [4a] G. Boche, A. Opel, M. Marsch, K. Harms, F. Haller, J. C. W. Lohrenz, C. Thümmler, W. Koch, *Chem. Ber.* **1992**, *125*, 2265. – [4b] G. Boche, F. Bosold, J. C. W. Lohrenz, A. Opel, P. Zulauf, *Chem. Ber.* **1993**, *126*, 1873.

[5] For Li/Hal carbenoids, see: G. Boche, M. Marsch, A. Müller, K. Harms, *Angew. Chem.* **1993**, *105*, 1081; *Angew. Chem. Int. Ed. Engl.* **1993**, *32*, 1032.

[6] For a review, see: E. Erdik, M. Ay, *Chem. Rev.* **1989**, *89*, 1947.

[7] [7a] N. I. Schverdina, Z. Kotscheschkov, *J. Gen. Chem. USSR (Engl. Transl.)* **1938**, *8*, 1825. – [7b] P. Beak, A. Basha, B.

Kokko, D. Loo, *J. Am. Chem. Soc.* **1986**, *108*, 6016. – [7c] J. P. Genet, S. Mallart, C. Greck, E. Piveteau, *Tetrahedron Lett.* **1991**, *32*, 2359. – [7d] G. Boche, C. Boie, F. Bosold, K. Harms, M. Marsch, *Angew. Chem.* **1994**, *106*, 90; *Angew. Chem. Int. Ed. Engl.* **1994**, *33*, 115.

[8] [8a] M. Nilsson, T. Norin, *Acta Chem. Scand.* **1963**, *17*, 1157. – [8b] P. Warner, S.-L. Lu, *J. Org. Chem.* **1976**, *41*, 1459. – [8c] E. J. Panek, L. R. Kaiser, G. M. Whitesides, *J. Am. Chem. Soc.* **1977**, *99*, 3708. – [8d] H. Neumann, D. Seebach, *Chem. Ber.* **1978**, *111*, 2785. – [8e] M. S. Kemp, R. S. Burden, R. S. T. Locffler, *J. Chem. Soc., Perkin Trans. 1* **1983**, 2267.

[9] R. D. Bach, M.-D. Su, J. L. Andrés, H. B. Schlegel, *J. Am. Chem. Soc.* **1993**, *115*, 8763.

[10] [10a] S. S. Woodard, M. G. Finn, K. B. Sharpless, *J. Am. Chem. Soc.* **1991**, *113*, 106. – [10b] M. G. Finn, K. B. Sharpless, *J. Am. Chem. Soc.* **1991**, *113*, 113.

[11] See, for example: [11a] H. Mimoun, P. Chaumette, M. Mignard, L. Saussine, J. Fischer, R. Weiss, *Nouv. J. Chim.* **1983**, *7*, 467. – [11b] A. van Asselt, B. D. Santarsiero, J. E. Bercaw, *J. Am. Chem. Soc.* **1986**, *108*, 8291. – [11c] S.-H. Zhao, O. Samuel, H. B. Kagan, *Tetrahedron* **1987**, *43*, 5135. – [11d] S. Campestrini, V. Conte, F. Di Furia, G. Modena, D. Bortolini, *J. Org. Chem.* **1988**, *53*, 5721. – [11e] G. Boche, K. Möbus, K. Harms, M. Marsch, *J. Am. Chem. Soc.* **1996**, *118*, 22770.

[12] Bond lengths given here are calculated at the BECKE3LYP/6-311G** level of theory.

[13] If not stated otherwise, all thermochemical data have been taken from: [13a] S. G. Lias, J. E. Bartmess, J. F. Liebman, J. L. Holmes, R. D. Levin, W. G. Mallard, *Gas-Phase Ion and Neutral Thermochemistry, J. Phys. Chem. Rev. Data*, Suppl. 1, **1988**. – [13b] S. G. Lias, J. F. Liebman, R. D. Levin, S. A. Kafafi, *NIST Standard Reference Database, Positive Ion Energetics*, Version 2.01, Gaithersburg, MD, **1994**. – [13c] J. E. Bartmess, *NIST Standard Reference Database, Negative Ion Energetics*, Version 3.01, Gaithersburg, MD, **1993**. – [13d] S. G. Lias, J. F. Liebman, R. D. Levin, *J. Phys. Chem. Ref. Data* **1984**, *13*, 695.

[14] For reviews on the mass spectrometry of anions, see: [14a] J. H. Bowie, *Mass Spectrom. Rev.* **1990**, *9*, 349. – [14b] O. Ingólfsson, F. Weik, E. Illenberger, *Int. J. Mass Spectrom. Ion Processes* **1996**, *155*, 1.

[15] K. L. Busch, G. L. Glish, S. A. McLuckey, *Mass Spectrometry/Mass Spectrometry: Techniques and Applications of Tandem Mass Spectrometry*, VCH Publishers, Weinheim, **1988**.

[16] For a discussion of the influence of high- and low-energy collisions and their use for structure elucidation, see: S. Chowdhury, A. G. Harrison, *J. Am. Chem. Soc.* **1988**, *110*, 7345.

[17] [17a] R. G. Cooks, J. H. Beynon, R. M. Caprioli, G. R. Lester, *Metastable Ions*, Elsevier, Amsterdam, **1973**. – [17b] R. D. Bowen, D. H. Williams, H. Schwarz, *Angew. Chem.* **1979**, *91*, 484; *Angew. Chem. Int. Ed. Engl.* **1979**, *18*, 451. – [17c] J. L. Holmes, J. K. Terlouw, *Org. Mass Spectrom.* **1980**, *15*, 383.

[18] For previous reports on dished topped peaks in the mass spectra of fragmenting anions, see: [18a] J. H. Bowie, B. D. Williams in: A. Maccoll (ed.), *Int. Rev. Sci. Mass Spectrom., Phys. Chem. Ser. 2*, Vol. 5, **1976**, p. 89. – [18b] J. H. Bowie, *Mass Spectrom. Rev.* **1984**, *3*, 161. – [18c] M. J. Raftery, J. H. Bowie, *Int. J. Mass. Spectrom. Ion Processes* **1988**, *85*, 167. – [18d] P. C. H. Eichinger, J. H. Bowie, R. N. Hayes, *J. Am. Chem. Soc.* **1989**, *111*, 4224. – [18e] G. W. Adams, J. H. Bowie, R. N. Hayes, *J. Chem. Soc., Perkin Trans. 2*, **1989**, 2159. – [18f] R. J. Waught, R. N. Hayes, P. C. H. Eichinger, K. M. Downard, J. H. Bowie, *J. Am. Chem. Soc.* **1990**, *112*, 2537. – [18g] P. C. H. Eichinger, J. H. Bowie, *J. Chem. Soc., Perkin Trans. 2* **1990**, 1763. – [18h] G. W. Adams, J. H. Bowie, R. N. Hayes, *J. Chem. Soc., Perkin Trans. 2* **1991**, 1809. – [18i] G. W. Adams, J. H. Bowie, R. N. Hayes, *Int. J. Mass Spectrom. Ion Processes* **1992**, *114*, 163.

[19] J. L. Holmes, A. A. Mommers, C. de Koster, W. Heerma, J. K. Terlouw, *Chem. Phys. Lett.* **1985**, *115*, 437.

[20] C. A. Schalley, D. Schröder, H. Schwarz, *Int. J. Mass Spectrom. Ion Processes* **1996**, *153*, 173.

[21] G. Herzberg, *Molecular Spectra and Molecular Structure – I. Spectra of Diatomic Molecules*, Krieger, Malabar (Florida), **1989**.

[22] J. M. Galbraith, H. F. Schaefer III, *J. Chem. Phys.* **1996**, *105*, 862.

[23] [23a] For a study on water oxide, see: D. Schröder, C. A. Schalley, N. Goldberg, J. Hrušák, H. Schwarz, *Chem. Eur. J.* **1996**, *2*, 1235. – [23b] A study of methanol and dimethyl ether oxide is in preparation: C. A. Schalley, J. Harvey, D. Schröder, H. Schwarz, R. Wrobel, W. Sander, unpublished results.

[24] [24a] K. Fukui, *Acc. Chem. Res.* **1981**, *12*, 363. – [24b] C. Gonzalez, H. B. Schlegel, *J. Chem. Phys.* **1989**, *90*, 2154. – [24c] C. Gonzalez, H. B. Schlegel, *J. Phys. Chem.* **1990**, *94*, 5523.

[25] [25a] J. E. Baldwin, *J. Chem. Soc., Chem. Commun.* **1976**, 734. – [25b] J. E. Baldwin, J. Cutting, W. Dupont, L. Kruse, L. Silberman, R. C. Thomas, *J. Chem. Soc., Chem. Commun.* **1976**, 736. – [25c] J. E. Baldwin, *J. Chem. Soc., Chem. Commun.* **1976**, 738. – [25d] H. B. Bürgi, J. D. Dunitz, *Acc. Chem. Res.* **1983**, *16*, 153. – [25e] C. D. Johnson, *Acc. Chem. Res.* **1993**, *26*, 476.

[26] The ion intensity of metastably generated $[2 - H_2]^-$ ions was much too low for characterizing the product ion by MI/CA experiments.

[27] Singe-point calculations at the BECKE3LYP/6-311++G** level of theory.

[28] The anion radical of CO_2 has been studied earlier: [28a] R. N. Compton, P. W. Reinhardt, C. D. Copper, *J. Phys. Chem.* **1975**, *63*, 3821. – [28b] A. Knapp, O. Echt, D. Kreisle, T. D. Märk, E. Recknagel, *Chem. Phys. Lett.* **1986**, *126*, 225.

[29] For earlier studies of carboxylates and isomeric ions, see, for example: [29a] P. C. Burgers, J. L. Holmes, J. E. Szuleiko, *Int. J. Mass Spectrom. Ion Processes* **1984**, *57*, 159. – [29b] D. Antolovic, V. J. Shiner, E. R. Davidson, *J. Am. Chem. Soc.* **1988**, *110*, 1375. – [29c] P. G. Wenthold, R. R. Squires, *J. Am. Chem. Soc.* **1994**, *116*, 11890, and literature cited therein. – [29d] A. Rauk, D. Yu, D. A. Armstrong, *J. Am. Chem. Soc.* **1994**, *116*, 8222. – [29e] D. Yu, A. Rauk, D. A. Armstrong, *J. Chem. Soc., Perkin Trans. 2* **1994**, 2207.

[30] [30a] G. E. Hartwell, T. L. Brown, *Inorg. Chem.* **1966**, *5*, 1257. – [30b] E. Weiss, H. Alsdorf, H. Kühr, H.-F. Grützmacher, *Chem. Ber.* **1968**, *101*, 3777. – [30c] J. E. Campana, B. N. Green, *J. Am. Chem. Soc.* **1984**, *106*, 531. – [30d] For a review of solid state structures of alkali alkoxides, see: E. Weiss, *Angew. Chem.* **1993**, *105*, 1565; *Angew. Chem. Int. Ed. Engl.* **1993**, *32*, 1501. – [30e] Also, see: T. Greiner, E. Weiss, *Chem. Ber.* **1977**, *110*, 3388.

[31] Larger clusters may also be formed with minimal intensities. However, they have not been observed in our EI mass spectra of lithium *tert*-butoxide.

[32] The third peak in the CA mass spectrum (Figure 10) may be an artifact, because the CA mass spectrum was recorded with ions mass selected by $B(1)$ only. See also figure caption and ref.[43].

[33] [33a] A. Opel, unpublished results **1991**. – [33b] See also the "dimerization" of $LiCHCl_2$ to give 1,2-dichloroethene: G. Köbrich, H. R. Merkle, *Chem. Ber.* **1966**, *99*, 1782. – [33c] Analogous reactions have been observed for α-lithiated ethers. See: A. Opel, Ph. D. Thesis, Universität Marburg, **1993**. – [33d] Also see: P. Kocienski, S. Wadman, K. Cooper, *J. Am. Chem. Soc.* **1989**, *111*, 2363.

[34] The decomposition reactions of hydrotrioxides have been studied earlier by experimental as well as theoretical means: [34a] J. Koller, M. Hodošcek, B. Plesnicar, *J. Am. Chem. Soc.* **1990**, *112*, 2124. – [34b] B. Plesnicar, J. Cerkovnik, J. Koller, F. Kovac, *J. Am. Chem. Soc.* **1991**, *113*, 4946. – [34c] B. Plesnicar in: W. Ando (ed.), *Organic Peroxides*, Wiley, New York, **1992**. – [34d] J. Cerkovnik, B. Plesnicar, *J. Am. Chem. Soc.* **1993**, *115*, 12169.

[35] G. Boche, K. Möbius, N. Schmiedebug, C. Bender, H. D. Brauer, unpublished results.

[36] It should be noted that the losses of oxygen atoms as well as molecular oxygen may be hampered additionally by barriers. These have, however, not been studied theoretically here.

[37] B. T. Lüke, J. A. Pople, P. v. R. Schleyer, T. Clark, *Chem. Phys. Lett.* **1983**, *102*, 148.

[38] C. A. Schalley, A. Fiedler, G. Hornung, R. Wesendrup, D. Schröder, H. Schwarz, *Chem. Eur. J.*, **1997**, *3*, 626.

[39] C. A. Schalley, M. Dieterle, D. Schröder, H. Schwarz, E. Uggerud, *Int. J. Mass Spectrom. Ion Processes*, in press.

[40] C. A. Schalley, R. Wesendrup, D. Schröder, T. Weiske, H. Schwarz, *J. Am. Chem. Soc.* **1995**, *117*, 7711.

[41] [41a] R. Srinivas, D. Sülzle, T. Weiske, H. Schwarz, *Int. J. Mass Spectrom. Ion Processes* **1991**, *107*, 368. – [41b] R. Srinivas, D. Sülzle, W. Koch, C. H. DePuy, H. Schwarz, *J. Am. Chem. Soc.* **1991**, *113*, 5970.

[42] [42a] C. E. Melton, *Principles of Mass Spectrometry and Negative Ions*, Dekker, New York, **1970**. – [42b] J. R. Chapman, *Practical Organic Mass Spectrometry*, Wiley, New York, **1985**. – [42c] S. T. Graul, R. R. Squires, *J. Am. Chem. Soc.* **1990**, *112*, 2506. –

[42d] S. T. Graul, R. R. Squires, *J. Am. Chem. Soc.* **1990**, *112*, 2517. – [42e] For a review on gas-phase stabilities of small anions, see: J. Kalcher, A. F. Sax, *Chem. Rev.* **1994**, *94*, 2291.
[43] D. Schröder, H. Schwarz, *Int. J. Mass Spectrom. Ion Processes* **1995**, *146/147*, 183.
[44] A. Rieche, F. Hitz, *Ber. Dtsch. Chem. Ges.* **1929**, *62*, 2458.
[45] P. G. Cookson, A. G. Davies, B. P. Roberts, *J. Chem. Soc., Chem. Commun.* **1976**, 1022.
[46] M. J. Frisch, G. W. Trucks, H. B. Schlegel, P. M. W. Gill, B. G. Johnson, M. A. Robb, J. R. Cheeseman, T. Keith, G. A. Peterson, J. A. Montgomery, K. Raghavachari, M. A. Al-Laham, V. G. Zakrzewski, J. V. Ortiz, J. B. Foresman, C. Y. Peng, P. Y. Ayala, W. Chen, M. W. Wong, J. L. Andres, E. S. Replogle, R. Gomperts, R. L. Martin, D. J. Fox, J. S. Binkley, D. J. Defrees, J. Baker, J. P. Stewart, M. Head-Gordon, C. Gonzales, J. A. Pople, *GAUSSIAN 94*, Revision B 3; GAUSSIAN Inc., Pittsburgh PA, **1995**.
[47] [47a] L. A. Curtis, K. Raghavachari, G. W. Trucks, J. A. Pople, *J. Chem. Phys.* **1991**, *94*, 7221. – [47b] L. A. Curtis, K. Raghavachari, J. A. Pople, *J. Chem. Phys.* **1993**, *98*, 1293. – [47c] For a modification of the G2 approach using DFT, see: C. W. Bauschlicher, Jr., H. Partridge, *J. Chem. Phys.* **1995**, *103*, 1788.
[48] R. Krishnan, J. S. Binkley, R. Seeger, J. A. Pople, *J. Chem. Phys.* **1980**, *72*, 650.
[49] [49a] G. Rauhut, R. Pulay, *J. Phys. Chem.* **1995**, *99*, 3093. – [49b] A. P. Scott, L. Radom, *J. Phys. Chem.* **1996**, *100*, 16502.
[50] P. M. W. Gill, B. G. Johnson, J. A. Pople, *Chem. Phys. Lett.* **1992**, *197*, 499.

[97067]